Developmental Biology 406 (2015) 259–270

Contents lists available at ScienceDirect

Developmental Biology

journal homepage: www.elsevier.com/locate/developmentalbiology

H^+/K^+ ATPase activity is required for biomineralization in sea urchin embryos

Daphne Schatzberg [a], Matthew Lawton [a], Sarah E. Hadyniak [a], Erik J. Ross [a], Tamara Carney [a], Wendy S. Beane [b], Michael Levin [c], Cynthia A. Bradham [a,*]

[a] Department of Biology, Boston University, Boston, MA 02215, USA
[b] Department of Biological Sciences, Western Michigan University, Kalamazoo, MI 49008, USA
[c] Department of Biology, Tufts University, Medford, MA 02155, USA

ARTICLE INFO

Article history:
Received 28 April 2015
Received in revised form
26 July 2015
Accepted 13 August 2015
Available online 15 August 2015

Keywords:
Sea urchin embryo
Bioelectricity
Skeletogenesis
SCH28080

ABSTRACT

The bioelectrical signatures associated with regeneration, wound healing, development, and cancer are changes in the polarization state of the cell that persist over long durations, and are mediated by ion channel activity. To identify physiologically relevant bioelectrical changes that occur during normal development of the sea urchin *Lytechinus variegatus*, we tested a range of ion channel inhibitors, and thereby identified SCH28080, a chemical inhibitor of the H^+/K^+ ATPase (HKA), as an inhibitor of skeletogenesis. In sea urchin embryos, the primary mesodermal lineage, the PMCs, produce biomineral in response to signals from the ectoderm. However, in SCH28080-treated embryos, aside from randomization of the left-right axis, the ectoderm is normally specified and differentiated, indicating that the block to skeletogenesis observed in SCH28080-treated embryos is PMC-specific. HKA inhibition did not interfere with PMC specification, and was sufficient to block continuing biomineralization when embryos were treated with SCH28080 after the initiation of skeletogenesis, indicating that HKA activity is continuously required during biomineralization. Ion concentrations and voltage potential were abnormal in the PMCs in SCH28080-treated embryos, suggesting that these bioelectrical abnormalities prevent biomineralization. Our results indicate that this effect is due to the inhibition of amorphous calcium carbonate precipitation within PMC vesicles.

1. Introduction

Bioelectricity refers to long-term changes in the voltage potential of cells, and the effect of these changes on biological systems (Levin, 2012, 2014). Bioelectricity plays a role in many processes, including wound healing (Nuccitelli, 2003; Nuccitelli et al., 2011; Wood, 2012), regeneration (Adams et al., 2007; Beane et al., 2011; Nogi et al., 2005), and the development of organisms as diverse as insects (Cole and Woodruff, 1997, 2000; Woodruff and Telfer, 1980), sea urchins (Akasaka et al., 1997; Fujino et al., 1987; Hibino et al., 2006; Mitsunaga et al., 1987), zebrafish (Kawakami et al., 2005; Nuckels et al., 2009), frogs, and chicks (Adams et al., 2006; Fukumoto et al., 2005; Levin et al., 2002). Ion channels are an excellent target for chemical inhibition, which is a relatively simple way to uncover their roles in biological processes. To elucidate further roles for bioelectrical changes in embryonic development, we screened various ion channel and pump inhibitors for effects on the development of sea urchin embryos, and found that inhibition of the H^+/K^+ ATPase (HKA) blocks skeletogenesis in embryos of the sea urchin *Lytechinus variegatus*.

The embryonic skeleton is secreted by the primary mesenchyme cells (PMCs). PMCs ingress into the blastocoel, then migrate into a stereotypical pattern within the blastocoel. The PMCs are arranged in a posterior ring around the blastopore with ventrolateral clusters that extend cords toward the anterior. PMCs are directed to these positions by ectodermal cues (Armstrong et al., 1993; Duloquin et al., 2007; Guss and Ettensohn, 1997); they subsequently secrete the skeleton in a pattern that conforms to this arrangement. Prior to the initiation of skeletogenesis, the PMCs fuse, forming a continuous syncytial cable (Hodor and Ettensohn, 1998), and the skeletal biomineral is deposited into an extracellular space surrounded by this syncytial membrane (Wilt et al., 2008).

The sea urchin skeleton is composed of the calcium carbonate mineral calcite and numerous associated proteins. The calcium in the skeleton is taken up from sea water (Nakano et al., 1963; Wilt et al., 2008) and carbonate is absorbed from sea water or generated by cellular metabolism (Stumpp et al., 2012). At least 40

* Corresponding author.
E-mail address: cbradham@bu.edu (C.A. Bradham).

http://dx.doi.org/10.1016/j.ydbio.2015.08.014
0012-1606/

distinct skeletal matrix proteins are embedded in the skeletal mineral in sea urchin larvae (Livingston et al., 2006; Wilt et al., 2008); however, little is known about their specific functions. The process of and mechanisms underlying biomineralization remain incompletely understood, and the sea urchin offers a relatively simple model in which to study this complex biological process.

The HKA is best known for its role in gastric acid secretion in mammals (Sachs et al., 1976). Activity of this pump has also been implicated in patterning of the left-right axis in frog, zebrafish, and chicken embryos (Gros et al., 2009; Kawakami et al., 2005; Levin et al., 2002; Mendes et al., 2014), and in signaling events that mediate head regeneration and regenerative tissue remodeling in planaria (Beane et al., 2011, 2013; Nogi et al., 2005). Discriminating the closely related HKA and NKA genes on the basis of sequence alone is extremely challenging, and HKA genes have not been identified in any sea urchin species to date. Chemical inhibitors offer a means to evaluate the functional role of this ion pump during sea urchin development. In this study, we show that HKA activity is required for precipitation of amorphous calcium carbonate within PMC vesicles, establishing the mechanistic basis for the block to biomineralization observed in HKA-inhibited embryos.

2. Results

2.1. SCH28080 is a potent inhibitor of skeletogenesis in the sea urchin larva

We identified SCH28080, a competitive inhibitor of the HKA

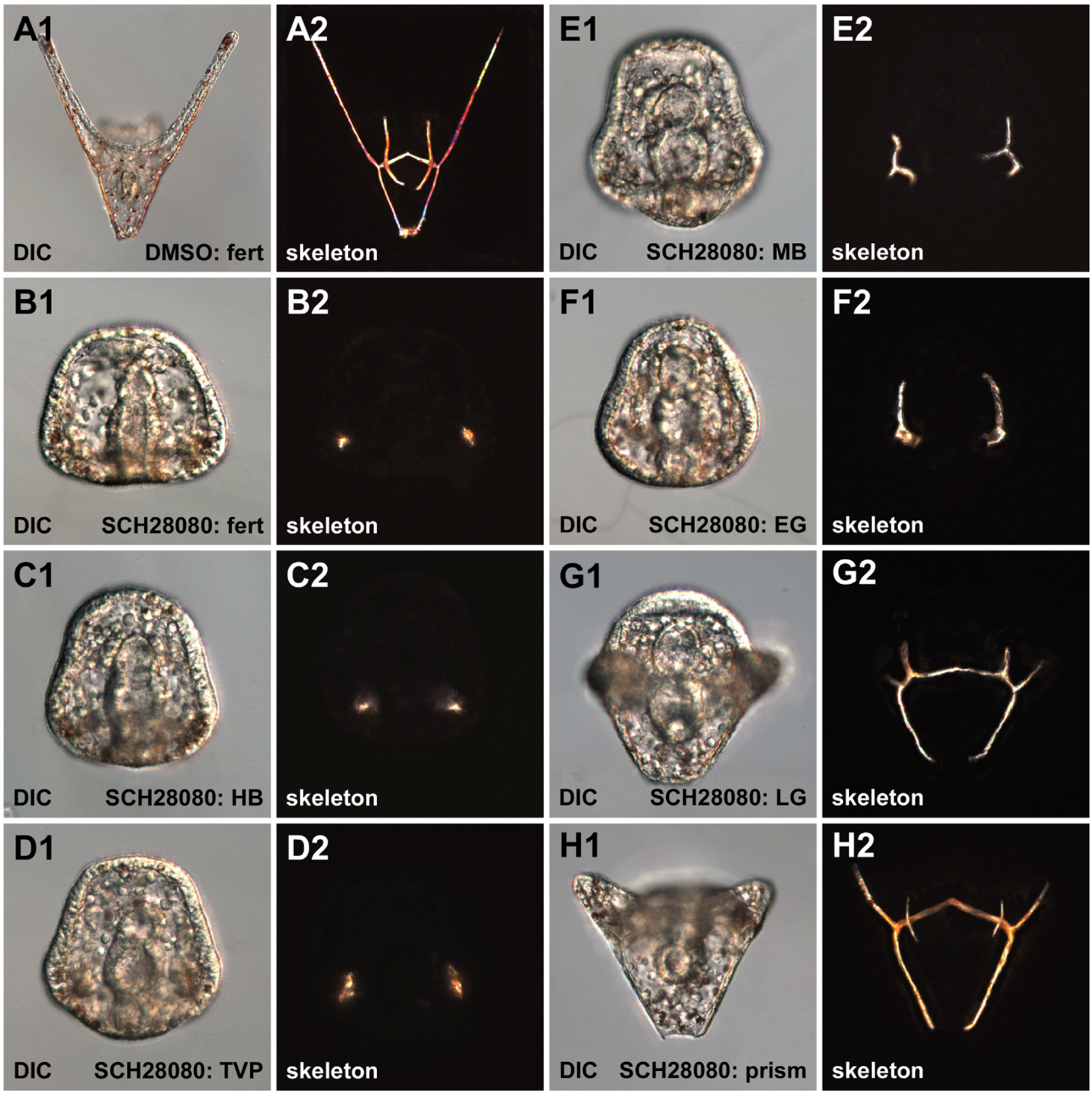

Fig. 1. SCH28080 treatment inhibits skeletogenesis. *Lytechinus variegatus* embryonic (DIC, 1) and skeletal (birefringence, 2) morphology is shown at late pluteus larva stage (48 h post-fertilization) after treatment with either vehicle (A) or SCH28080 (B–H) at the indicated developmental stages. Abbreviations: Fert – fertilization; HB – hatched blastula; TVP – thickened vegetal plate; MB – mesenchyme blastula; EG – early gastrula; LG – late gastrula.

(Abe et al., 2011; Beil et al., 1986; Vagin et al., 2002), as an inhibitor of skeletogenesis in sea urchin larvae (Fig. 1A-B). SCH28080 is highly specific and does not inhibit the closely related Na^+/K^+ ATPase (NKA) (Lyu and Farley, 1997). Consistent with this, skeletal growth was similarly prevented in embryos treated with Omeprazole, another HKA inhibitor with a distinct mechanism of action (Morii et al., 1990), while Ouabain, an inhibitor of the closely related NKA, had no effect on skeletogenesis (Fig. S1). When SCH28080 was added to *Lytechinus variegatus* (Lv) cultures prior to PMC ingression (Fig. 1B–D), the resulting larvae initiated small skeletal spicules, as evidenced by bilateral birefringent dots at the normal sites of skeletogenesis in the PMC clusters. However, these spicules failed to elongate or branch to produce a normal skeleton. The most conspicuous defect in these embryos is the lack of skeletal elongation; gastrulation appears to be normal (Fig. 1B–D). After PMC ingression, embryos were not as sensitive to SCH28080 treatment, and were capable of making some amount of primary skeleton (Fig. 1E–F). SCH28080 treatment after the initiation of skeletogenesis resulted in stunted but morphologically normal skeletons (Fig. 1G–H). These results show that SCH28080 treatment blocks skeletogenesis even after it has been initiated, indicating that SCH28080 inhibits processes that are active during biomineralization. The minimum effective dose of SCH28080 for preventing skeletogenesis in Lv embryos is 125 μM, which is markedly higher than the 50 μM dose reported to randomize the left/right axis in another sea urchin species (Hibino et al., 2006). In our model, a 50 μM dose of SCH28080 was not sufficient to prevent skeletogenesis (Fig. S1C), although it did increase the incidence of left/right axis defects to 40% of embryos, compared to 12% of control embryos (Fig. S2C–F). The higher dose of 125 μM increased the incidence of left/right axis defects further, to 61% of embryos (Fig. S2G–J).

2.2. Specification and differentiation of the ectoderm are unaffected in SCH28080-treated embryos

PMCs receive skeletal patterning information and biomineralization cues from the ectoderm (Armstrong et al., 1993; Duloquin et al., 2007; Guss and Ettensohn, 1997). Thus, a key question is whether the lack of skeletogenesis in SCH28080-treated embryos results from defects in the ectoderm. Fluorescent in-situ hybridization (FISH) experiments were performed to assess the specification of the ectoderm using well-characterized genes in the ectoderm gene regulatory network (GRN) (Ben-Tabou de-Leon et al., 2013; Li et al., 2012; Saudemont et al., 2010; Su et al., 2009) (Fig. 2). At late gastrula stage, *chordin* (Bradham et al., 2009), *irxA* (McIntyre et al., 2013), *lefty* (Duboc et al., 2008), and *tbx2/3* (Gross, 2003) expression was unchanged in SCH28080-treated embryos compared to controls (Figs. 2A1-A2, B1-B2), indicating that dorsal-ventral ectodermal specification is normal in SCH28080-treated embryos. VEGF is a growth factor secreted from the ectoderm which is required for biomineralization (Duloquin et al., 2007). Spatial expression of VEGF and its receptor, here referred to as VEGFR, were unaffected in SCH28080-treated embryos compared to DMSO-treated controls (Fig. S3). These results were corroborated by QPCR analysis (Fig. S4A-B). Together, these data indicate that ectodermal dorsal-ventral specification and VEGF signaling are not perturbed in SCH28080-treated embryos.

To evaluate ectodermal differentiation, we labeled the ciliary band and neurons in SCH28080-treated larvae (Fig. 2B3–B4). The ciliary band is a default ectodermal state, and is spatially restricted to a stripe between the dorsal and ventral territories via repression by TGFß-mediated dorsal and ventral specification (Yaguchi et al., 2010) (Fig. 2A3). In SCH28080-treated embryos, the ciliary band is a tightly restricted stripe (Fig. 2B3), indicating that the ectodermal dorsal-ventral specification occurs normally in embryos treated with SCH28080. Neural development in the sea urchin larva is a relatively late event indicative of ectodermal differentiation (Burke, 1978). Synaptotagmin B (synB) is a pan-neural marker that labels neurons positioned along the ciliary band (Fig. 2A4, red), while a subset of anterior neurons are serotonergic (Fig. 2A4, green). Both types of neurons are normally positioned in SCH28080-treated embryos (Fig. 2B4), indicating that neural differentiation and patterning are not impacted by SCH28080. Thus, neither the specification nor differentiation of the ectoderm is

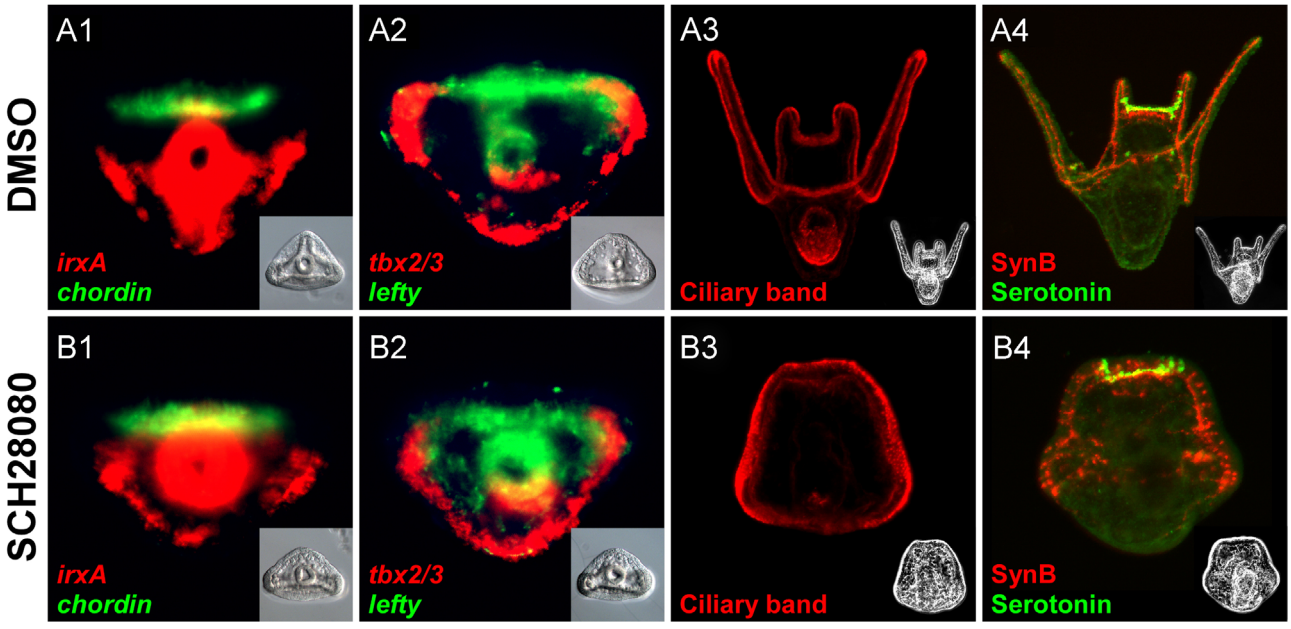

Fig. 2. Ectoderm dorsal-ventral specification and differentiation is not perturbed by SCH28080 treatment. Embryos treated with either vehicle (A) or SCH28080 (B) were fixed at late gastrula stage and subjected to fluorescent in situ hybridization (FISH) for dorsal IrxA (A1, B1) or Tbx2/3 (A2, B2) and ventral Chordin (A1, B1) or Lefty (A2, B2). Embryos fixed at pluteus stage were stained for the ciliary band (A3, B3) or the neural markers synaptotagmin B (A4, B4, red), which labels all neurons, and serotonin (A4, B4, green). Insets show the corresponding DIC or phase contrast images; all embryos are presented in vegetal views with ventral toward the top, except in B3, which is an en face ventral view.

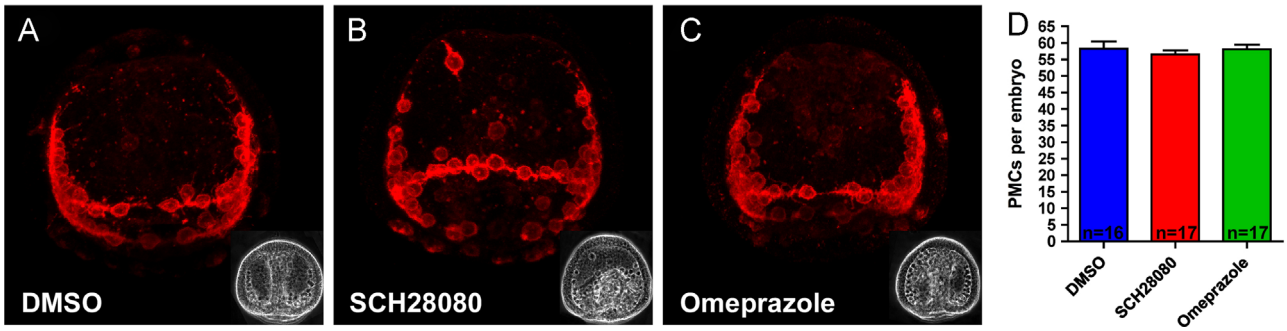

Fig. 3. PMC positioning is normal in SCH28080- and Omeprazole-treated embryos. Vehicle- (A), SCH28080- (B), and Omeprazole-treated embryos (C) were fixed at late gastrula stage and immunolabeled for PMCs. The corresponding phase contrast images are inset. The number of PMCs per embryo is shown for each treatment as average ± SEM.

perturbed in SCH28080-treated embryos.

2.3. SCH28080 treatment impairs PMC syncytium formation but not PMC specification

At late gastrula stage, the PMCs in control embryos arrange themselves in a posterior ring around the blastopore, with ventrolateral clusters that extend cords toward the anterior (Fig. 3A). Embryos treated with SCH28080 (Fig. 3B) or Omeprazole (Fig. 3C) also have a PMC ring-and-cords structure, although a few PMCs exhibit perturbed positioning in each case. The number of PMCs per embryo was not affected by either SCH28080 or Omeprazole treatment (Fig. 3D), demonstrating that HKA inhibition does not affect the number or positioning of PMCs at late gastrula stage.

We next assessed PMC syncytium formation by expressing GFP in half of the PMCs, then determining whether the marker spread to the remaining PMC complement (Fig. 4A). In vehicle-treated embryos, GFP co-labeled nearly every PMC (Fig. 4B1–B3). In contrast, only 50% of the PMCs from the uninjected side of the SCH28080-treated embryos became GFP positive (Fig. 4C1–C3), indicating that syncytium formation is impaired by SCH28080 treatment; further, this effect was reproducible (Fig. 4D). Thus, SCH28080 treatment partially inhibits PMC syncytium formation.

Given the effects on biomineralization and syncytium formation, we next evaluated the expression of members of the PMC gene regulatory network (Rafiq et al., 2012). Surprisingly, no changes in localization or expression levels of these genes was detected by in situ hybridization or qPCR analysis in SCH28080-treated embryos (Fig. S4C,S5). We included several biomineralization genes, and these were also unaffected by SCH28080 (Fig. S4D). These results demonstrate that the known PMC specification and differentiation networks are intact in SCH28080-treated embryos.

2.4. PMC ion distributions are perturbed by SCH28080 treatment

We expected to observe bioelectrical changes in embryos treated with SCH28080, because this drug acts as an ion pump inhibitor. To confirm and quantitate those effects, we used a range of fluorescent probes to detect cellular polarity and relative ion concentrations (Fig. 5A-B). Measurements were taken at a range of time points comprising PMC ingression, PMC migration, and gastrulation. First, relative polarization was measured using the voltage-sensitive dye bis-(1,3-dibutylbarbituric acid)trimethine oxonol ($DiBAC_4(3)$), or DiBAC (Adams and Levin, 2012; Epps et al., 1994). The overall voltage potential in control PMCs exhibits only

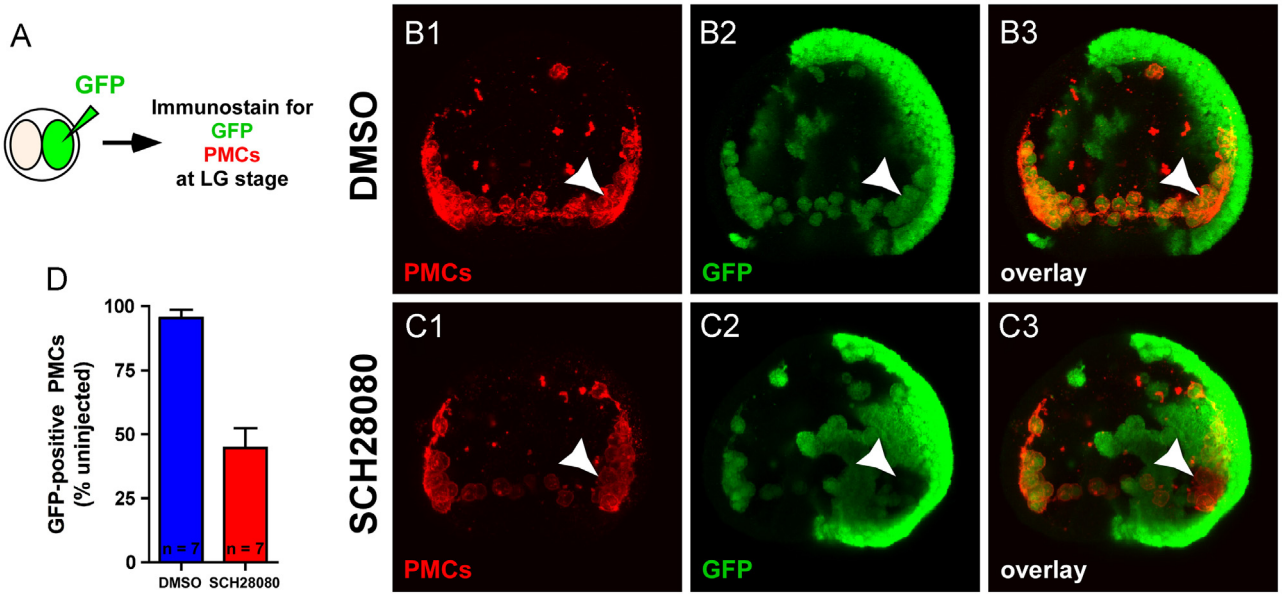

Fig. 4. PMC syncytium formation is impaired in SCH28080-treated embryos. A. Schematic of the experimental design. B., C. Control (B) and SCH28080-treated embryos (C) were immunolabeled for PMCs (1) and GFP (2); overlays are shown in panel 3. Partial projections of each confocal z-stack are shown for clarity. Arrowhead indicates a cluster of PMCs, which are GFP-negative in the SCH28080-treated embryo. D. The number of uninjected GFP-positive PMCs (i.e., PMCs that fused) is reduced by approximately 50% with SCH28080 treatment, shown as average ± SEM.

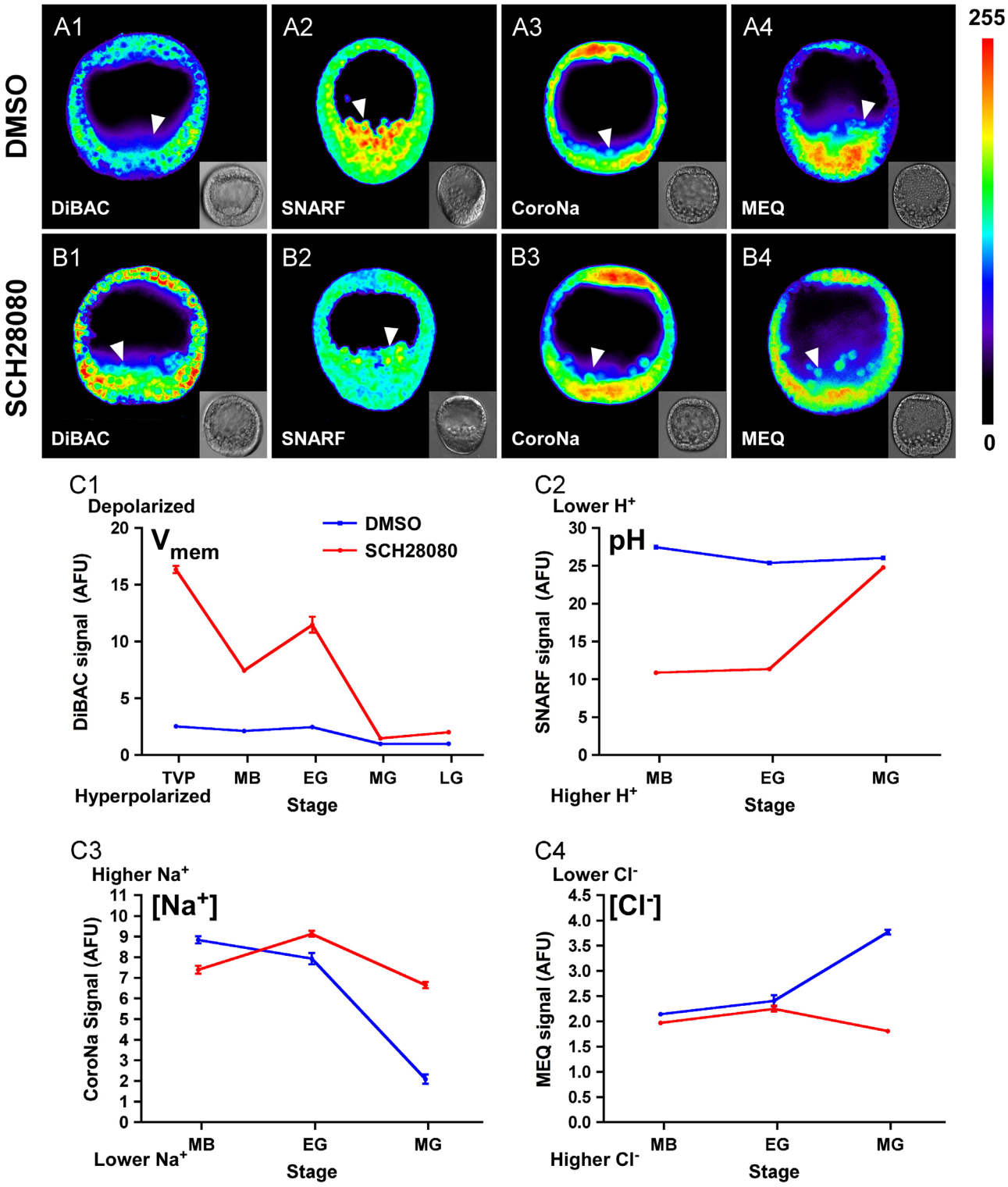

Fig. 5. SCH28080 treatment depolarizes PMCs and modulates ion concentrations. Exemplars of vehicle- (A) and SCH28080-treated (B) embryos at mesenchyme blastula stage, and quantitative results (C) are shown for the indicator dyes DiBAC, which senses voltage (1), SNARF, which senses protons (2), CoroNa, which senses sodium ions (3), and MEQ, which senses chloride ions (4). A., B. All panels are presented as single *z* slices from a confocal microscope with the indicated look-up-table applied. Arrow-heads indicate PMCs. Insets show the corresponding phase images. C. The fluorescence signal intensity within PMCs of vehicle- (blue) or SCH28080-treated (red) embryos is plotted at the indicated developmental stages, as averages ± SEM; the relative values are given in arbitrary fluorescence units (AFU). Each data point represents measurements from 12 or more embryos, with the exception of three control points, which were measured in fewer embryos. Note that the *y*-axis in C4 is inverted, with low signal corresponding to high chloride ion concentrations, since Cl^- ions quench MEQ fluorescence. Abbreviations are as in Fig. 1.

minor changes through the end of gastrulation (Fig. 5C1). The PMCs in SCH28080-treated embryos are dramatically depolarized compared to those in vehicle-treated embryos (Fig. 5A1, B1, C1). This effect is pronounced at the early timepoints from thickened vegetal plate through early gastrula stages, corresponding to the ingression and migration of the PMCs. However, as gastrulation proceeds, the polarization state of the PMCs in SCH28080-treated embryos becomes comparable to that in controls (Fig. 5C1). Proton

distributions were measured using the pH-sensitive dye 5-(and-6)-carboxy SNARF®-1 acetoxymethyl ester acetate (SNARF) (Bassnett et al., 1990; Buckler and Vaughan-Jones, 1990; Han and Burgess, 2010). Control PMCs have a consistent pH over time, while the PMCs in SCH28080-treated embryos have a relatively acidic pH, or high proton concentration, at mesenchyme blastula and early gastrula stages (Fig. 5A2, B2, C2). This is as expected, since SCH28080 inhibits an H^+ exchanger. Although the HKA is an electroneutral ion pump, it often works in tandem with K^+ efflux channels to modulate membrane voltage (Aw et al., 2008; Beane et al., 2011; Fujita et al., 2002; Lambrecht et al., 2005; Shibata et al., 2006). The change in proton levels is thus consistent with and can account for the relative depolarization observed at these stages in SCH28080-treated embryos (Fig. 5C1). At midgastrula stage, the pH is comparable between SCH28080-treated embryos and controls, again matching the overall polarization changes as measured by DiBAC. Finally, sodium and chloride ion concentrations were measured by the dyes CoroNa Green AM (CoroNa) and 6-methoxy-N-ethylquinolinium iodide (MEQ), respectively (Biwersi and Verkman, 1991; Martin et al., 2005; Meier et al., 2006; Woll et al., 1996). In control embryos, both sodium and chloride ion levels decline following early gastrula stage. Both ions were present at comparable levels in the PMCs of SCH28080-treated and control embryos at early time points (Fig. 5A3–A4, B3-B4, C3-C4). However, at mid-gastrula stage, neither ion concentration declined in SCH28080-treated embryos (Fig. 5C3–C4). Thus, relative depolarization and proton concentration are increased during PMC ingression and migration in SCH28080-treated embryos. Sodium and chloride ion concentrations increased (relative to controls) only later as gastrulation proceeds, and concomitant with the recovery of normal polarization and pH in SCH28080-treated embryos, suggesting that the later changes in sodium and

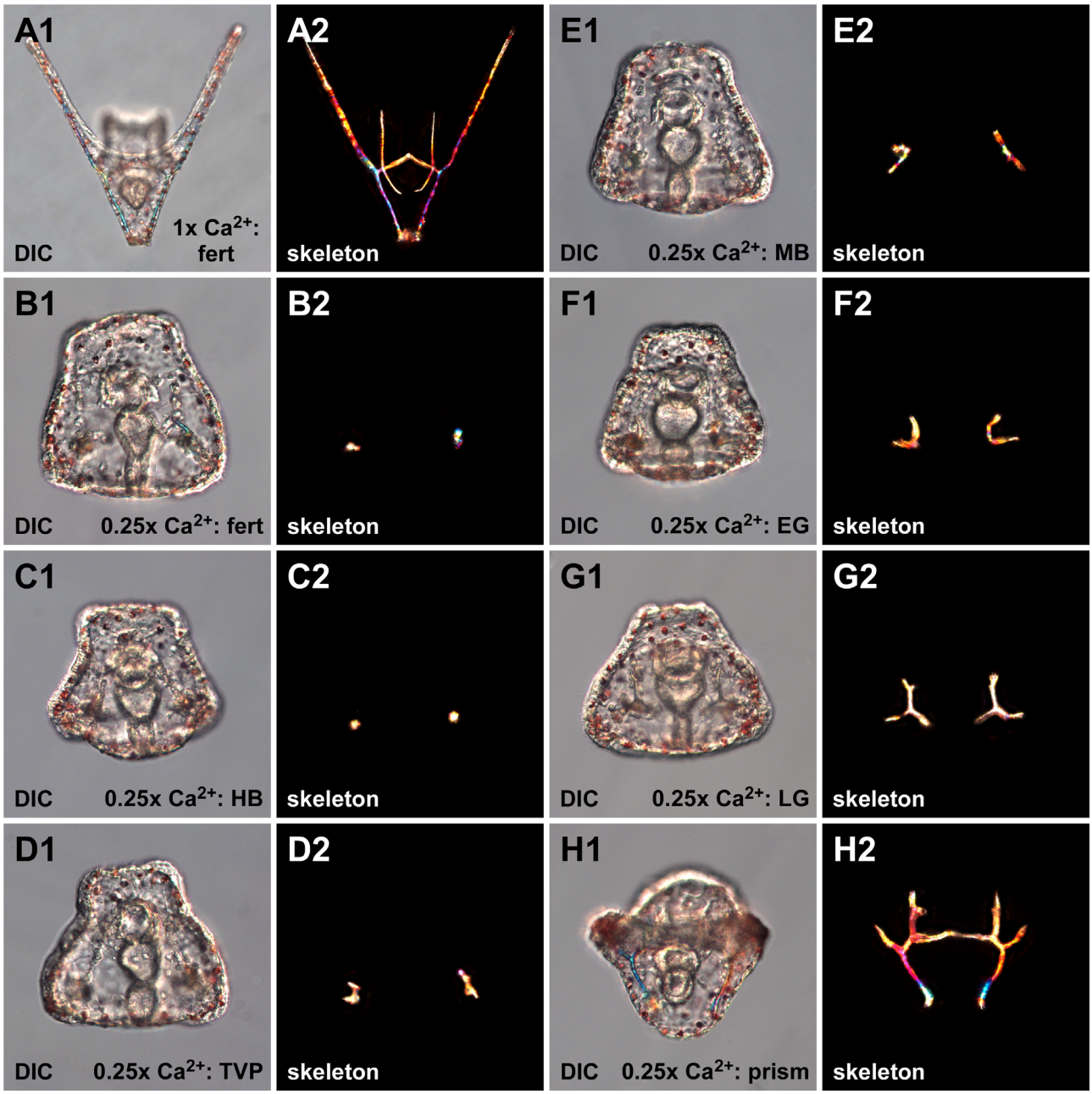

Fig. 6. Low-calcium sea water phenocopies SCH28080-treatment. Embryonic (DIC, 1) and skeletal morphology (plane polarized light, 2) is shown at pluteus stage after washing into artificial sea water with normal (A) or reduced (B–H) levels of calcium at the indicated developmental stages. Abbreviations as in Fig. 1.

chloride ions are compensatory. Measurements of relative polarization and ion concentrations were also made for the ectoderm (Fig. S6), and this tissue exhibits profiles that are similar to those observed in the PMCs in both vehicle- and SCH28080-treated embryos, indicating that SCH28080 affects ion distributions throughout the embryo, and not solely in the PMCs. These data suggest that the HKA is broadly expressed, and also indicate that ectodermal dorsal-ventral specification and differentiation is relatively refractory to these changes in ion concentrations.

2.5. SCH28080 treatment is phenotypically consistent with insufficient calcium availability

SCH28080 treatment impairs skeletogenesis even when added to embryos after the initiation of skeletogenesis (Fig. 1G-H), implying that SCH28080 treatment directly impacts the biomineralization process. One obvious possibility is that SCH28080 treatment blocks calcium import into the embryo. Consistent with this possibility, the effect of SCH28080 treatment is phenocopied by developing embryos in sea water that contains 25% of the normal calcium concentration (Fig. 6). Lower sea water calcium concentrations were not compatible with embryo survival, possibly due to disruption of cadherins junctions (data not shown). Interestingly, washing embryos into low-calcium sea water at different developmental stages resulted in effects similar to treating with SCH28080 at those same stages (compare Fig. 6 with Fig. 1). Neither of these treatments results in an abrupt halt to skeletogenesis; instead, biomineralization continues for a few hours,

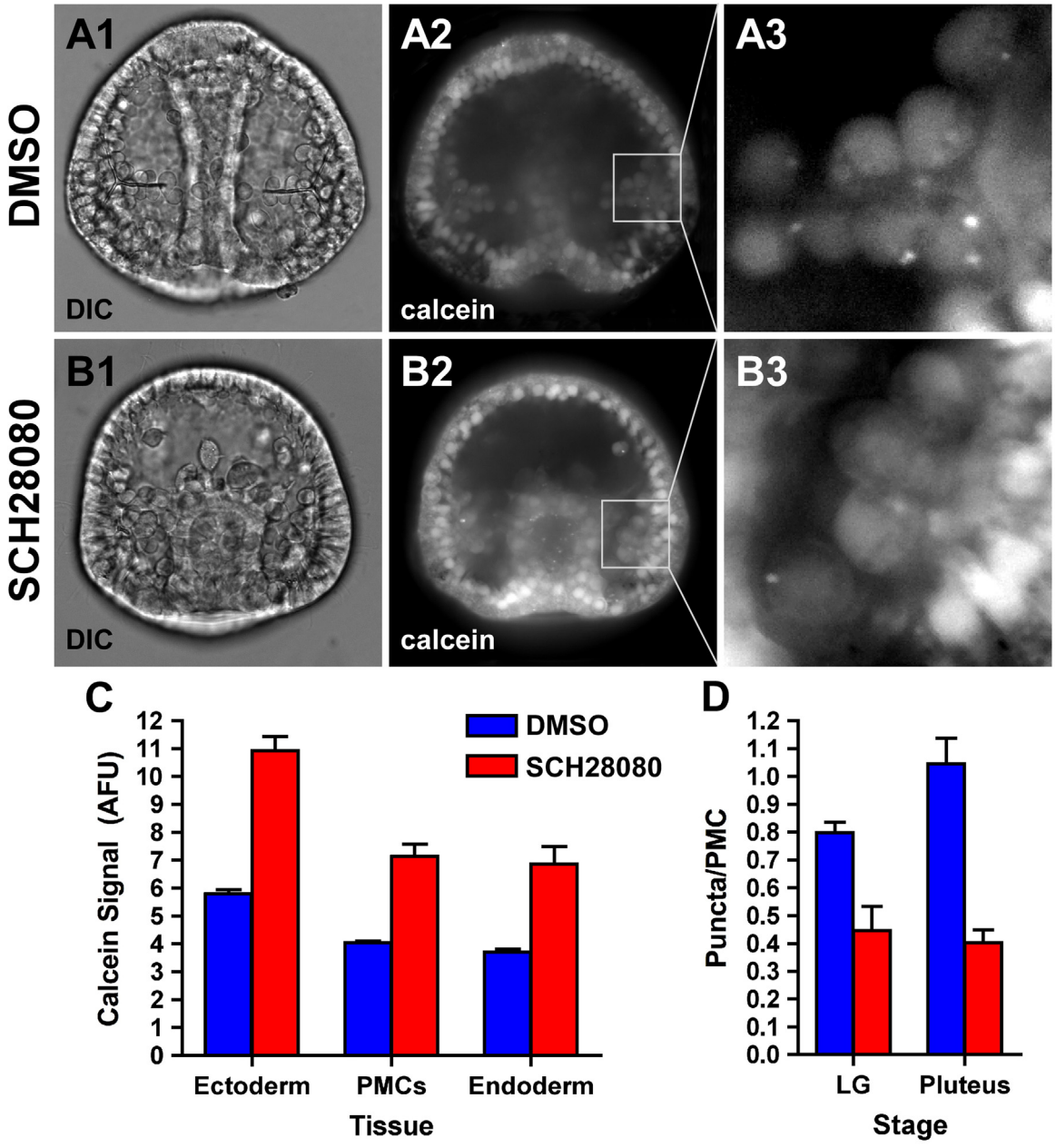

Fig. 7. SCH28080treatment results in increased calcium levels in embryonic tissues, and decreased numbers of calcium-rich puncta in the PMCs. A., B. Examples of vehicle- (A) and SCH28080-treated (B) embryos imaged with the calcium-sensitive fluorescent dye calcein are shown as DIC images (1), confocal images of single z-slices of calcein fluorescence (2), and magnified views of the indicated region (3). In magnified views, the contrast has been increased to clarify the puncta. C. Quantitation of calcein fluorescence levels in the indicated tissues of late gastrula (LG) stage embryos treated with vehicle or SCH28080, shown as average arbitrary fluorescence units (AFU) ± SEM. D. Numbers of puncta per PMC in vehicle- or SCH28080-treated embryos at the indicated stages, shown as average counts ± SEM.

consistent with an interval during which intracellular calcium stores may be depleted (Wilt et al., 2008). We thus hypothesized that SCH28080 treatment prevents calcium accumulation in the PMCs, thereby blocking skeletogenesis. We tested this hypothesis by co-treating embryos with SCH28080 and the calcium ionophore A23187, which permits free movement of calcium ions across cell membranes. However, rather than rescuing the effects of SCH28080, A23187 treatment had little if any impact on spicule initiation in SCH28080-treated embryos and slightly retarded skeletogenesis at high doses in controls (Fig. S7). These results contradict the hypothesis and indicate that SCH28080 does not block calcium import.

2.6. PMCs in embryos treated with SCH28080 have increased intracellular calcium concentrations, but reduced numbers of calcium-rich puncta

We next asked how calcium concentrations are affected in SCH28080-treated embryos using the calcium-sensitive fluorescent dye calcein AM (Pinsino et al., 2011; Vidavsky et al., 2014; Wilt et al., 2008) (Fig. 7). Surprisingly, SCH28080-treated embryos reproducibly possess relatively elevated calcium levels in all tissues (Fig. 7A–C). Bright calcein puncta are visible within the PMCs of control embryos (Fig. 7A3), which correspond to calcium-rich vesicles that contain nanospheres of amorphous calcium carbonate (ACC) (Vidavsky et al., 2014). SCH28080-treated embryos have approximately half the number of puncta per PMC as control embryos at late gastrula stage, when skeletogenesis is initiating (Fig. 7A3, B3, D). This difference was more pronounced at pluteus stage, since control embryos had increased numbers of puncta per PMC, while SCH28080-treated embryos did not (Fig. 7D). These data indicate that SCH28080 treatment, despite generally elevating calcium levels, blocks the accumulation of ACC vesicles in PMCs. These results also imply that the reduced number of ACC vesicles observed in the PMCs within SCH28080-treated embryos is insufficient to support biomineralization.

3. Discussion

In this study, we use ion pump inhibitors to show that activity of the HKA is required for skeletogenesis in the sea urchin embryo. We demonstrate that treatment with the HKA inhibitor SCH28080 impairs PMC syncytium formation and prevents skeletogenesis. Addition of the drug after the initiation of skeletogenesis is sufficient to prevent further growth of the skeleton, indicating that ongoing HKA activity is required during biomineralization.

The randomization of the left-right axis we observed at low doses of the inhibitor is consistent with previous studies using SCH28080 and other HKA inhibitors in sea urchins (Duboc et al., 2005; Hibino et al., 2006). The block to skeletogenesis at higher doses was replicated in this study with Omeprazole, another HKA inhibitor, and this phenotype is also consistent with previous studies of HKA inhibition in sea urchins (Fujino et al., 1987; Mitsunaga et al., 1987). Although there are some concerns about non-specific effects of SCH28080 on the NKA (Lyu and Farley, 1997), NKA inhibition in the present study using Ouabain did not result in a block to skeletogenesis in Lv embryos. Moreover, the effects we observe are consistent with a specific effect on HKA activity, since proton levels, but not sodium or chloride levels, are rapidly responsive to SCH28080. Pre-gastrular SCH28080-treated embryos have a relatively high proton concentration compared to controls. This matches the relative depolarization exhibited by SCH28080-treated embryos compared to controls at these timepoints. During gastrulation, proton concentration and overall polarization in SCH28080-treated embryos become comparable to controls, while sodium and chloride concentrations are increased in SCH28080-treated embryos compared to controls. Because the NKA is expressed throughout the development of the embryo (data not shown), it is unlikely that these relatively late changes to Na^+ and Cl^- concentrations represent off-target effects of the drug, and we therefore interpret these late effects on sodium and chloride ions as reflecting compensatory changes by which SCH28080-treated embryos restore voltage and pH homeostasis. Interestingly, despite the normal proton concentrations and voltage potential of SCH28080-treated embryos at the end of gastrulation when skeletogenesis initiates, these embryos remain unable to undergo biomineralization.

The voltage and ion concentration changes we observed in SCH28080-treated embryos were present in the ectoderm as well as the PMCs. Our results indicate that voltage changes in the ectoderm do not disrupt dorsal-ventral specification. Based on the expression of in situ markers, ciliary band and neural labeling, and the appearance of bilateral spicule initiations, ectodermal dorsal-ventral specification and neural development appears to be normal in SCH28080-treated embryos. In contrast, in situs for left-right markers indicate randomization of the left-right axis in embryos treated with SCH28080, consistent with previous studies (Duboc et al., 2005; Hibino et al., 2006). The results indicate that the effects of HKA-mediated changes in voltage potential within the ectoderm are limited to left-right axis specification.

SCH28080- and Omeprazole-treated embryos exhibit a strong block to biomineralization, which prompted us to evaluate VEGF and VEGFR expression, since this signal-receptor pair is required for biomineralization (Adomako-Ankomah and Ettensohn, 2013; Duloquin et al., 2007; Knapp et al., 2012). Surprisingly, we found that VEGF and VEGFR expression was normal in SCH28080-treated embryos. This interesting result indicates that normal VEGF and VEGFR expression is not sufficient for skeletogenesis in embryos lacking HKA activity. These results are consistent with a model in which HKA activity functions downstream from VEGF signaling within the PMCs, although it is also possible that the HKA operates independently of VEGF.

Because we observed a complete loss of skeleton in embryos treated with SCH28080 prior to PMC ingression, we measured biomineralization genes such as SM30, SM50, and p16 (Cheers and Ettensohn, 2005; Wilt et al., 2013; Wilt, 1999; Wilt et al., 2008), and found that biomineralization genes are expressed at normal levels in SCH28080-treated embryos. These unexpected results indicate, first, that PMC specification does not require HKA activity, and second, that biomineralization gene expression does not suffice for skeletogenesis. Because syncytium formation was inhibited in SCH28080-treated embryos and the PMC GRN factor Twist is required for PMC fusion (Wu et al., 2008), we assessed Twist expression, and found that Twist levels are also comparable in SCH28080-treated and control embryos. In fact, we found no differences in the expression of any genes in the well-described PMC specification gene regulatory network in SCH28080-treated embryos. It remains unclear how syncytium formation is impaired by HKA inhibition, but our results indicate that it is not via modulation of the known PMC GRN. In comparison to the GRN describing PMC specification, the PMC differentiation GRN is relatively sparse. Aside from Twist, no genes are known that impact PMC fusion; thus, it is possible that SCH28080 inhibits the expression of a currently unknown suite of PMC fusion genes. Thus, chemical approaches that inhibit ion channels and pumps as used in the present study may serve to highlight biological processes for which portions of the GRN are relatively incomplete. Alternatively, it is plausible that the defect in PMC fusion in SCH28080-treated embryos reflects a direct biophysical constraint on the fusion process itself, which may require a relatively hyperpolarized state within the PMCs.

In the absence of both Twist and syncytium formation, skeletogenesis is profoundly blocked (Wu et al., 2008); thus, it is possible that the impaired PMC fusion in SCH28080-treated embryos contributes to the block to skeletogenesis therein, particularly in embryos treated with SCH28080 prior to the fusion event. However, defective fusion cannot account for the inhibition of biomineralization that occurs with SCH28080 treatment initiated subsequent to syncytium formation.

Importantly, addition of SCH28080 after skeletogenesis has begun prevents further biomineralization. Thus, biomineralization requires continuous HKA activity. Notably, the block to skeletogenesis occurs with a delay, which suggests that the embryo becomes depleted of a component required for biomineralization. While loss of external calcium phenocopies SCH28080 treatment by also producing a delayed block to skeletogenesis, addition of a calcium ionophore did not rescue SCH28080 treatment, indicating that decreased calcium uptake does not explain the lack of skeleton production in SCH28080-treated embryos. We found, instead, that SCH28080 treatment results in increased intracellular calcium ion levels in the PMCs, along with decreased numbers of calcium-rich puncta. These puncta represent vesicles of precipitated amorphous calcium carbonate (ACC) that is destined for secretion onto the mineral matrix (Vidavsky et al., 2014). Thus, calcium ions are stalled within PMCs in SCH28080-treated embryos, and are unable to be precipitated and exported to the skeleton, accounting for the block to biomineralization observed with HKA inhibition.

Intracellular precipitation of ACC generates protons, and requires a buffering mechanism to proceed (McConnaughey and Whelan, 1997; Stumpp et al., 2012). The mechanism used to buffer this reaction in sea urchins has not been elucidated, although it has been suggested that the HKA may play a role (Fujino et al., 1987; Mitsunaga et al., 1987; Stumpp et al., 2012). Importantly, we have shown that SCH28080-mediated acidification of the intracellular pH within PMCs is transient and returns to control levels before skeletogenesis initiates (Fig. 5C2); thus, it seems unlikely that PMC acidification can account directly for the block to ACC precipitation. We also found that SCH28080 treatment provokes a delayed increase in sodium and chloride ions (Fig. 5C3–C4). It is possible that these late ion imbalances impair carbonate transport, and that defective carbonate transport underlies the block to ACC precipitation observed with HKA inhibition. Carbonate ions are transported into cells largely by two mechanisms. Anion exchangers exchange carbonate and chloride ions in an electroneutral manner, while co-transporters mediate the movement of carbonate and sodium ions in an electrogenic manner, in a ratio of greater than 1:1 (sodium:carbonate). These are both passive processes, relying on existing ion gradients of sodium and chloride to drive transport of carbonate ions (Romero et al., 2013; Soleimani, 2013). Thus, it is likely that bicarbonate ion concentrations are perturbed in SCH28080-treated embryos, but it is unclear whether they are increased or decreased, and to what extent.

Human biomineralization shares many commonalities with the process in sea urchins. Osteoblasts secrete collagen and other matrix proteins to form a scaffold (Blair et al., 2011; van de Peppel and van Leeuwen, 2014). Precipitation of hydroxyapatite, a calcium phosphate mineral, begins in vesicles which bud from osteoblasts to deliver mineral to the protein scaffold (Anderson, 2003). Precipitation of bone mineral releases protons, and requires a slightly alkaline pH to proceed (Blair et al., 2011). It remains unknown how osteoblasts buffer sites of biomineralization. Recent evidence shows that adults on long-term HKA inhibitor therapy have an elevated risk of osteoporosis, suggesting that biomineralization is impaired by HKA inhibition (Fournier et al., 2009; Targownik et al., 2008; Vestergaard et al., 2006; Yang et al., 2006). An important question to address is whether this HKA-inhibitor-mediated defect in biomineralization in humans results from acidification at the site of biomineral precipitation, or from imbalances in other ions such as sodium and chloride, as is the case in the sea urchin embryo.

4. Conclusions

Bioelectrical changes are critical for many aspects of collective cellular biology, including wound healing, regeneration, and developmental axis specification. Here we show that a normal bioelectrical signature is required for biomineralization of the sea urchin larval skeleton by the skeletogenic primary mesenchyme cells (PMCs). Inhibition of the H^+/K^+ ATPase (HKA) during sea urchin development prevents biomineralization of the calcium carbonate endoskeleton. The PMCs normally form a syncytium prior to skeletogenesis, and HKA inhibition impairs but does not block syncytium formation. However, the defect in syncytium formation cannot be responsible for the block to biomineralization, since HKA activity is required continuously as biomineral is produced.

We show that HKA inhibition blocks the intravesicular precipitation of amorphous calcium carbonate (ACC). Although the precipitation of ACC is thought to be pH dependent, we show that HKA inhibition results in only a transient decrease in intracellular pH and concomitant depolarization of the PMCs. At the developmental stages when biomineral is precipitated, pH homeostasis is restored in the PMCs, while intracellular levels of sodium and chloride ions are increased; we interpret these changes as compensatory. We show that HKA inhibition does not impair calcium uptake, but does inhibit ACC precipitation. We speculate that this effect is mediated through perturbed uptake of carbonate ions secondary to the compensatory changes in sodium and chloride ion concentrations. These results show that bioelectrical homeostasis is required to support ACC precipitation and biomineralization. Importantly, we show that pH homeostasis alone is not sufficient to support biomineralization; this novel result indicates that other ions must be maintained at appropriate levels for biomineralization to proceed. The question remains whether this requirement for bioelectrical homeostasis is conserved in other organisms that undergo biomineralization.

5. Materials and methods

5.1. Embryo culture, microinjection, drug treatments, and photography

Adult *Lytechinus variegatus* were obtained from either Reeftopia (Florida) or the Duke University Marine Labs (North Carolina). Gametes were harvested and zygotic microinjections were performed by standard methods. mRNA was prepared using the mMessage mMachine Kit (Ambion). SCH28080, Omeprazole, Ouabain, and A23187 (Sigma) were resuspended in anhydrous DMSO and added to cultures before the second cleavage unless otherwise indicated. Dose-response experiments determined that a minimum effective dose of 125 μM SCH28080 was necessary to prevent skeletogenesis. This dose varied slightly with different populations of embryos and different preparations of drug. Calcium-free sea water was prepared (450 mM sodium chloride, 9 mM potassium chloride, 48 mM magnesium sulfate, 6 mM sodium bicarbonate) and mixed proportionally with normal artificial sea water (480 mM sodium chloride, 10 mM potassium chloride, 26 mM magnesium chloride hexahydrate, 28 mM magnesium sulfate, 14 mM calcium chloride, 2 mM sodium bicarbonate) for

low-calcium sea water treatments. Embryos were imaged on an Zeiss Axioplan microscope at 200 × with DIC optics or with plane-polarized light to visualize birefringent skeletons. In some cases, the latter images are shown as montages of different focal planes to depict the entire skeleton in focus.

5.2. In situ hybridization

In situ hybridization was carried out by standard methods. Probes for LvChordin, LvTbx2/3, LvIrxA, LvVEGF, LvVEGFR, and LvSoxE were previously described (Bradham et al., 2009; Gross, 2003; McIntyre et al., 2013; Piacentino et al., 2015; Walton et al., 2009). Probes for LvLefty, LvPitx2, LvAlx1, LvErg, LvEts, LvFoxB, LvSnail, LvTbr, and LvTwist were kind gifts from Dave McClay. Sequences for these genes except LvLefty and LvPitx2 were previously described (Saunders and McClay, 2014). A full-length probe for LvFoxO was generated from Lv late gastrula stage cDNA. Probes were labeled with either digoxigenin (Roche) or DNP-11-UTP (Perkin Elmer). Visualization was carried out either with BM Purple (Roche) or with Tyramide Signal Amplification Plus kit (Perkin Elmer) using either fluorescein or Cy3. Embryos were imaged on a Zeiss Axioplan microscope.

5.3. QPCRs

Total RNA was collected from cultures of DMSO- and SCH28080-treated embryos at either hatched blastula or late gastrula stage. RNA was isolated with Trizol (Life Technologies) and precipitated with glycogen carrier (Ambion). Samples were DNAse-treated (DNA-free, Ambion) before reverse transcription using the TaqMan Reverse Transcription kit (Life Technologies). QPCR was performed with SYBR Green PCR Master Mix (Applied Biosystems) in an ABI 7900ht qPCR thermocycler. Each bar presented represents three biological replicates (each in triplicate, nine total measurements). C_T values were normalized to LvSetmar expression, and are presented as average ± SE relative to control. Primer sequences are presented in Table ST1.

5.4. Immunofluorescence

Immunofluorescent labeling was performed as previously described (Bradham et al., 2009). Primary antibodies were 295 (ciliary band), 1e11 (synaptotagmin B), anti-serotonin (Sigma), 6a9 (PMCs), and anti-GFP (Torrey Pines Biolabs). Secondary antibodies from Jackson Labs were either Cy2 or Cy3 conjugated. Embryos were imaged on an Olympus Fv10i laser scanning confocal microscope. Z-stacks were projected using Olympus software and full projections are presented except in the case of Fig. 4, where partial projections are shown to increase clarity.

5.5. Ion dyes and quantitations

A panel of fluorescent ion-indicator dyes was used to assess ion distributions. Bis-(1,3-dibutylbarbituric acid)trimethine oxonol ($DiBAC_4(3)$) (DiBAC, relative polarization), 5-(and-6)-carboxy SNARF®-1 acetoxymethyl ester acetate (SNARF, pH), CoroNa Green AM (CoroNa, sodium), 6-methoxy-N-ethylquinolinium iodide (MEQ, chloride), and Calcein AM (calcein, calcium) were purchased from Invitrogen. Dyes were used according to the manufacturer's instructions and embryos were imaged live on either an Olympus Fv10i laser scanning confocal, Olympus DSU spinning disk confocal, or Olympus Fv1000 scanning confocal. Raw 16 bit images of single z-slices were quantitated using a custom Matlab script. Each image was normalized to background fluorescence levels by sampling empty space at the corners of the image and dividing all other signal intensities by this "zero" value. All comparisons were made between groups of embryos imaged on the same microscope with identical image acquisition settings. DiBAC measurements were taken independently at each time point for matched groups of vehicle- and SCH28080-treated embryos and the results were normalized to a time-course of control embryos acquired with consistent imaging parameters. SNARF images were collected at two emission wavelengths, 580 nm and 640 nm. Raw images were thresholded such that any pixel containing less than 0.5% of the maximum intensity was set to 0. The ratio of the two images was made using a custom ImageJ plugin created by modifying Ratio Plus. The custom plugin defines any pixel equal to 0 for which either the numerator or denominator is 0. This generated a ratio image, which was quantitated in Matlab. Because the thresholding step created images for which the background signal equaled 0, the normalization-to-background step was omitted. Error bars shown are standard errors.

Author contributions

D.S., M. Levin and C.A.B. designed, and D.S., M. Lawton, S.E.H., E. J.R, T.C. and W.S.B. performed the experiments in this study. D.S. and C.A.B. wrote the manuscript.

Conflict of interest

None.

Acknowledgments

We thank Eva Fast for an initial Matlab script used for processing voltage and ion dye images, and Jessica Keenan for the final version of that script; Lindsay Saunders and David McClay for clones of several PMC GRN genes; Robert Burke, David McClay, and Chuck Ettensohn for gifts of antibodies; and Dr. Caren Eliezer for helpful discussions about the manuscript. E.J.R. and S.E.H. were partially supported by Boston University Undergraduate Research Opportunities Program fellowships. This study was supported by start-up funds from Boston University (C.A.B.).

Appendix A. Supplementary material

Supplementary data associated with this article can be found in the online version at http://dx.doi.org/10.1016/j.ydbio.2015.08.014.

References

Abe, K., Tani, K., Fujiyoshi, Y., 2011. Conformational rearrangement of gastric H(+),K(+)-ATPase induced by an acid suppressant. Nat. Commun. 2, 155.
Adams, D.S., Levin, M., 2012. Measuring resting membrane potential using the fluorescent voltage reporters DiBAC4(3) and CC2-DMPE. Cold Spring Harb Protoc 2012, 459–464.
Adams, D.S., Masi, A., Levin, M., 2007. H+ pump-dependent changes in membrane voltage are an early mechanism necessary and sufficient to induce Xenopus tail regeneration. Development 134, 1323–1335.
Adams, D.S., Robinson, K.R., Fukumoto, T., Yuan, S., Albertson, R.C., Yelick, P., Kuo, L., McSweeney, M., Levin, M., 2006. Early, H+-V-ATPase-dependent proton flux is necessary for consistent left-right patterning of non-mammalian vertebrates. Development 133, 1657–1671.
Adomako-Ankomah, A., Ettensohn, C.A., 2013. Growth factor-mediated mesodermal cell guidance and skeletogenesis during sea urchin gastrulation. Development 140, 4214–4225.
Akasaka, K., Uemoto, H., Wilt, F.H., Mitsunaga-Nakatsubo, K., Shimada, H., 1997. Oral-aboral ectoderm differentiation of sea urchin embryos is disrupted in response to calcium ionophore. DeV. Growth Differ. 39, 373.
Anderson, H.C., 2003. Matrix vesicles and calcification. Curr. Rheumatol. Rep. 5, 222.

Armstrong, N., Hardin, J., McClay, D., 1993. Cell-cell interactions regulate skeleton formation in the sea urchin embryo. Development 119, 833.
Aw, S., Adams, D.S., Qiu, D., Levin, M., 2008. H,K-ATPase protein localization and Kir4.1 function reveal concordance of three axes during early determination of left-right asymmetry. Mech. Dev. 125, 353–372.
Bassnett, S., Reinisch, L., Beebe, D.C., 1990. Intracellular pH measurement using single excitation-dual emission fluorescence ratios. Am. J. Physiol. 258, C171.
Beane, W.S., Morokuma, J., Adams, D.S., Levin, M., 2011. A chemical genetics approach reveals H,K-ATPase-mediated membrane voltage is required for planarian head regeneration. Chem. Biol. 18, 77–89.
Beane, W.S., Morokuma, J., Lemire, J.M., Levin, M., 2013. Bioelectric signaling regulates head and organ size during planarian regeneration. Development 140, 313–322.
Beil, W., Hackbarth, I., Sewing, K.F., 1986. Mechanism of gastric antisecretory effect of SCH 28080. Br. J. Pharmacol. 88, 19.
Ben-Tabou de-Leon, S., Su, Y.H., Lin, K.T., Li, E., Davidson, E.H., 2013. Gene regulatory control in the sea urchin aboral ectoderm: spatial initiation, signaling inputs, and cell fate lockdown. Dev. Biol. 374, 245–254.
Biwersi, J., Verkman, A.S., 1991. Cell-permeable fluorescent indicator for cytosolic chloride. Biochemistry 30, 7879.
Blair, H.C., Robinson, L.J., Huang, C.L., Sun, L., Friedman, P.A., Schlesinger, P.H., Zaidi, M., 2011. Calcium and bone disease. Biofactors 37, 159–167.
Bradham, C.A., Oikonomou, C., Kuhn, A., Core, A.B., Modell, J.W., McClay, D.R., Poustka, A.J., 2009. Chordin is required for neural but not axial development in sea urchin embryos. Dev. Biol. 328, 221–233.
Buckler, K.J., Vaughan-Jones, R.D., 1990. Application of a new pH-sensitive fluoroprobe (carboxy-SNARF-1) for intracellular pH measurement in small, isolated cells. Pflugers Arch 417, 234.
Burke, R.D., 1978. The structure of the nervous system of the pluteus larva of strongylocentrotus purpuratus. Cell Tissue Res. 191, 233.
Cheers, M.S., Ettensohn, C.A., 2005. P16 is an essential regulator of skeletogenesis in the sea urchin embryo. Dev. Biol. 283, 384–396.
Cole, R.W., Woodruff, R.I., 1997. Charge dependent distribution of endogenous proteins within vitellogenic ovarian follicles of actias luna. J. Insect Physiol. 43, 275–287.
Cole, R.W., Woodruff, R.I., 2000. Vitellogenic ovarian follicles of Drosophila exhibit a charge-dependent distribution of endogenous soluble proteins. J. Insect Physiol. 46, 1239–1248.
Duboc, V., Lapraz, F., Besnardeau, L., Lepage, T., 2008. Lefty acts as an essential modulator of Nodal activity during sea urchin oral-aboral axis formation. Dev. Biol. 320, 49–59.
Duboc, V., Rottinger, E., Lapraz, F., Besnardeau, L., Lepage, T., 2005. Left-right asymmetry in the sea urchin embryo is regulated by nodal signaling on the right side. Dev. Cell 9, 147–158.
Duloquin, L., Lhomond, G., Gache, C., 2007. Localized VEGF signaling from ectoderm to mesenchyme cells controls morphogenesis of the sea urchin embryo skeleton. Development 134, 2293–2302.
Epps, D.E., Wolfe, M.L., Groppi, V., 1994. Characterization of the steady-state and dynamic fluorescence properties of the potential-sensitive dye bis-(1,3-dibutylbarbituric acid)trimethine oxonol (Dibac4(3)) in model systems and cells. Chem. Phys. Lipids 69, 137.
Fournier, M.R., Targownik, L.E., Leslie, W.D., 2009. Proton pump inhibitors, osteoporosis, and osteoporosis-related fractures. Maturitas 64, 9–13.
Fujino, Y., Mitsunaga-Nakatsubo, K., Yasumasu, I., 1987. Inhibitory effect of omeprazole, a specific inhibitor of H+, K+-ATPase, on spicule formation in sea urchin embryos and in cultured micromere-derived cells. Development, Growth & Differentiation 29, 591.
Fujita, A., Horio, Y., Higashi, K., Mouri, T., Hata, F., Takeguchi, N., Kurachi, Y., 2002. Specific localization of an inwardly rectifying K+ channel, Kir4.1, at the apical membrane of rat gastric parietal cells; its possible involvement in K+ recycling for the H+-K+-pump. The Journal of Physiology 540, 85–92.
Fukumoto, T., Kema, I.P., Levin, M., 2005. Serotonin signaling is a very early step in patterning of the left-right axis in chick and frog embryos. Curr Biol 15, 794–803.
Gros, J., Feistel, K., Viebahn, C., Blum, M., Tabin, C.J., 2009. Cell movements at hensen's node establish left/right asymmetric gene expression in the chick. Science 324, 941.
Gross, J.M., 2003. LvTbx2/3: a T-box family transcription factor involved in formation of the oral/aboral axis of the sea urchin embryo. Development 130, 1989–1999.
Guss, K.A., Ettensohn, C.A., 1997. Skeletal morphogenesis in the sea urchin embryo: regulation of primary mesenchyme gene expression and skeletal rod growth by ectoderm-derived cues. Development 124, 1899.
Han, J., Burgess, K., 2010. Fluorescent indicators for intracellular pH. Chem. Rev. 110, 2709.
Hibino, T., Ishii, Y., Levin, M., Nishino, A., 2006. Ion flow regulates left-right asymmetry in sea urchin development. Dev. Genes Evol. 216, 265.
Hodor, P.G., Ettensohn, C.A., 1998. The dynamics and regulation of mesenchymal cell fusion in the sea urchin embryo. Dev. Biol. 199, 111.
Kawakami, Y., Raya, A., Raya, R.M., Rodriguez-Esteban, C., Belmonte, J.C.I., 2005. Retinoic acid signaling links left-right asymmetric patterning and bilaterally symmetric somitogenesis in the zebrafish embryo. Nature 435, 165.
Knapp, R.T., Wu, C.H., Mobilia, K.C., Joester, D., 2012. Recombinant sea urchin vascular endothelial growth factor directs single-crystal growth and branching in vitro. J. Am. Chem. Soc. 134, 17908–17911.
Lambrecht, N.W., Yakubov, I., Scott, D., Sachs, G., 2005. Identification of the K efflux channel coupled to the gastric H-K-ATPase during acid secretion. Physiol. Genomics 21, 81–91.
Levin, M., 2012. Molecular bioelectricity in developmental biology: new tools and recent discoveries: control of cell behavior and pattern formation by transmembrane potential gradients. Bioessays 34, 205–217.
Levin, M., 2014. Molecular bioelectricity: how endogenous voltage potentials control cell behavior and instruct pattern regulation in vivo. Mol. Biol. Cell 25, 3835–3850.
Levin, M., Thorlin, T., Robinson, K.R., Nogi, T., Mercola, M., 2002. Asymmetries in H+/K+-ATPase and cell membrane potentials comprise a very early step in left-right patterning. Cell 111, 77.
Li, E., Materna, S.C., Davidson, E.H., 2012. Direct and indirect control of oral ectoderm regulatory gene expression by Nodal signaling in the sea urchin embryo. Dev. Biol. 369, 377–385.
Livingston, B.T., Killian, C.E., Wilt, F., Cameron, A., Landrum, M.J., Ermolaeva, O., Sapojnikov, V., Maglott, D.R., Buchanan, A.M., Ettensohn, C.A., 2006. A genome-wide analysis of biomineralization-related proteins in the sea urchin Strongylocentrotus purpuratus. Dev. Biol. 300, 335–348.
Lyu, R.M., Farley, R.A., 1997. Amino acids Val115-Ile126 of rat gastric H+-K+-ATPase confer high affinity for Sch-28080 to Na+-K+-ATPase. Am. J. Physiol. 272, C1717.
Martin, V.V., Rothe, A., Gee, K.R., 2005. Fluorescent metal ion indicators based on benzoannelated crown systems: a green fluorescent indicator for intracellular sodium ions. Bioorg. Med. Chem. Lett. 15, 1851–1855.
McConnaughey, T.A., Whelan, J.F., 1997. Calcification generates protons for nutrient and bicarbonate uptake. Earth-Sci. Rev. 42, 95.
McIntyre, D.C., Seay, N.W., Croce, J.C., McClay, D.R., 2013. Short-range Wnt5 signaling initiates specification of sea urchin posterior ectoderm. Development 140, 4881–4889.
Meier, S.D., Kovalchuk, Y., Rose, C.R., 2006. Properties of the new fluorescent Na+ indicator CoroNa Green: comparison with SBFI and confocal Na+ imaging. J. Neurosci. Methods 155, 251–259.
Mendes, R.V., Martins, G.G., Cristovao, A.M., Saude, L., 2014. N-cadherin locks left-right asymmetry by ending the leftward movement of Hensen's node cells. Dev. Cell 30, 353–360.
Mitsunaa, K., Fujino, Y., Yasumasu, I., 1987. Probable role of allylisothiocyanate-sensitive H+, K+-ATPase in spicule calcification in embryos of the sea urchin Hemicentrotus pulcherrimus. Dev. Growth Differ. 29, 57.
Morii, M., Takata, H., Takeguchi, N., 1990. Binding site of omeprazole in hog gastric H+,K+-ATPase. Biochem. Biophys. Res. Commun. 167, 754.
Nakano, E., Okazaki, K., Iwamatsu, T., 1963. Accumulation of radioactive calcium in larvae of the sea urchin pseudocentrotus depressus. Biol. Bull. 125, 125.
Nogi, T., Yuan, Y.E., Sorocco, D., Perez-Tomas, R., Levin, M., 2005. Eye regeneration assay reveals an invariant functional left-right asymmetry in the early bilaterian Dugesia japonica. Laterality 10, 193.
Nuccitelli, R., 2003. Endogenous electric fields in embryos during development, regeneration and wound healing. Radiat. Prot. Dosimetry 106, 375.
Nuccitelli, R., Nuccitelli, P., Li, C., Narsing, S., Pariser, D.M., Lui, K., 2011. The electric field near human skin wounds declines with age and provides a noninvasive indicator of wound healing. Wound Repair Regen. 19, 645–655.
Nuckels, R.J., Ng, A., Darland, T., Gross, J.M., 2009. The vacuolar-ATPase complex regulates retinoblast proliferation and survival, photoreceptor morphogenesis, and pigmentation in the zebrafish eye. Invest Ophthalmol. Vis. Sci. 50, 893–905.
Piacentino, M.L., Ramachandran, J., Bradham, C.A., 2015. Late Alk4/5/7 signaling is required for anterior skeletal patterning in sea urchin embryos. Development 142, 943–952.
Pinsino, A., Roccheri, M.C., Costa, C., Matranga, V., 2011. Manganese interferes with calcium, perturbs ERK signaling, and produces embryos with no skeleton. Toxicol. Sci. 123, 217–230.
Rafiq, K., Cheers, M.S., Ettensohn, C.A., 2012. The genomic regulatory control of skeletal morphogenesis in the sea urchin. Development 139, 579–590.
Romero, M.F., Chen, A.P., Parker, M.D., Boron, W.F., 2013. The SLC4 family of bicarbonate (HCO(3)(-)) transporters. Mol. Aspects Med. 34, 159–182.
Sachs, G., Chang, H.H., Rabon, E., Schackman, R., 1976. A nonelectrogenic H+ pump in plasma membranes of hog stomach. J. Biol. Chem. 251, 7690.
Saudemont, A., Haillot, E., Mekpoh, F., Bessodes, N., Quirin, M., Lapraz, F., Duboc, V., Rottinger, E., Range, R., Oisel, A., et al., 2010. Ancestral regulatory circuits governing ectoderm patterning downstream of Nodal and BMP2/4 revealed by gene regulatory network analysis in an echinoderm. PLoS Genetics 6, e1001259.
Saunders, L.R., McClay, D.R., 2014. Sub-circuits of a gene regulatory network control a developmental epithelial-mesenchymal transition. Development 141, 1503–1513.
Shibata, T., Hibino, H., Doi, K., Suzuki, T., Hisa, Y., Kurachi, Y., 2006. Gastric type H+, K+-ATPase in the cochlear lateral wall is critically involved in formation of the endocochlear potential. Am. J. Physiol. Cell Physiol. 291, C1038–C1048.
Soleimani, M., 2013. SLC26 Cl-/HCO3- exchangers in the kidney: roles in health and disease. Kidney Int. 84, 657–666.
Stumpp, M., Hu, M.Y., Melzner, F., Gutowska, M.A., Dorey, N., Himmerkus, N., Holtmann, W.C., Dupont, S.T., Thorndyke, M.C., Bleich, M., 2012. Acidified seawater impacts sea urchin larvae pH regulatory systems relevant for calcification. Proc. Natl. Acad. Sci. 109, 18192.
Su, Y.H., Li, E., Geiss, G.K., Longabaugh, W.J., Kramer, A., Davidson, E.H., 2009. A perturbation model of the gene regulatory network for oral and aboral ectoderm specification in the sea urchin embryo. Dev. Biol. 329, 410–421.
Targownik, L.E., Lix, L.M., Metge, C.J., Prior, H.J., Leung, S., Leslie, W.D., 2008. Use of proton pump inhibitors and risk of osteoporosis-related fractures. Can. Med.

Assoc. J. 179, 319–326.
Vagin, O., Denevich, S., Munson, K., Sachs, G., 2002. SCH28080, a K+-competitive inhibitor of the gastric H,K-ATPase, binds near the M5-6 luminal loop, preventing K+ access to the ion binding domain. Biochemistry 41, 12755.
van de Peppel, J., van Leeuwen, J.P., 2014. Vitamin D and gene networks in human osteoblasts. Front Physiol. 5, 137.
Vestergaard, P., Rejnmark, L., Mosekilde, L., 2006. Proton pump inhibitors, histamine H2 receptor antagonists, and other antacid medications and the risk of fracture. Calcified Tissue Int. 79, 76–83.
Vidavsky, N., Addadi, S., Mahamid, J., Shimoni, E., Ben-Ezra, D., Shpigel, M., Weiner, S., Addadi, L., 2014. Initial stages of calcium uptake and mineral deposition in sea urchin embryos. Proc. Natl. Acad. Sci. USA 111, 39–44.
Walton, K.D., Warner, J., Hertzler, P.H., McClay, D.R., 2009. Hedgehog signaling patterns mesoderm in the sea urchin. Dev. Biol. 331, 26–37.
Wilt, F., Killian, C.E., Croker, L., Hamilton, P., 2013. SM30 protein function during sea urchin larval spicule formation. J. Struct. Biol. 183, 199–204.
Wilt, F.H., 1999. Matrix and mineral in the sea urchin larval skeleton. J. Struct. Biol. 126, 216.
Wilt, F.H., Killian, C.E., Hamilton, P., Croker, L., 2008. The dynamics of secretion during sea urchin embryonic skeleton formation. Exp Cell Res 314, 1744–1752.
Woll, E., Gschwentner, M., Furst, J., Hofer, S., Buemberger, G., Jungwirth, A., Frick, J., Deetjen, P., Paulmichl, M., 1996. Fluorescence-optical measurements of chloride movements in cells using the membrane-permeable dye diH-MEQ. Pflugers Arch. 432, 486.
Wood, W., 2012. Wound healing: calcium flashes illuminate early events. Curr. Biol. 22, R14–R16.
Woodruff, R.I., Telfer, W.H., 1980. Electrophoresis of proteins in intercellular bridges. Nature 286, 84.
Wu, S.Y., Yang, Y.P., McClay, D.R., 2008. Twist is an essential regulator of the skeletogenic gene regulatory network in the sea urchin embryo. Dev. Biol. 319, 406–415.
Yaguchi, S., Yaguchi, J., Angerer, R.C., Angerer, L.M., Burke, R.D., 2010. TGFbeta signaling positions the ciliary band and patterns neurons in the sea urchin embryo. Dev. Biol. 347, 71–81.
Yang, Y.X., Lewis, J.D., Epstein, S., Metz, D.C., 2006. Long-term proton pump inhibitor therapy and risk of hip fracture. J. Am. Med. Assoc. 296, 2947.